



Contents lists available at ScienceDirect

Arabian Journal of Chemistry

journal homepage: www.sciencedirect.com

Original article

Study of montmorillonite modification technology using polyvinylpyrrolidone

Volodymyr Krasinskyi^{a,b,*}, Rafał Malinowski^a, Krzysztof Bajer^a, Piotr Rytlewski^c, Andrzej Miklaszewski^d

^aLukasiewicz Research Network – Institute for Engineering of Polymer Materials and Dyes, 55 M. Skłodowska-Curie Street, Toruń 87-100, Poland

^bLviv Polytechnic National University, Department of Chemical Technology of Plastics Processing, Bandera 12 St., 79013 Lviv, Ukraine

^cKazimierz Wielki University, Faculty of Materials Engineering, 30 Chodkiewicza Street, Bydgoszcz 85-064, Poland

^dPoznan University of Technology, Institute of Material Science and Engineering, Jana Pawła II 24, 60-965 Poznan, Poland

ARTICLE INFO

Article history:

Received 8 May 2023

Accepted 20 September 2023

Available online 25 September 2023

Keywords:

Montmorillonite
Polyvinylpyrrolidone
Structure
Intercalation
Exfoliation
Flocculation

ABSTRACT

In this work, a new method of modifying montmorillonite (Mt) with polyvinylpyrrolidone (PVP) was developed, which makes it possible to obtain modified Mt with different structures and modifier content simultaneously. The essence of the method consists in mixing colloidal solutions of Mt and PVP, processing the mixture with ultrasound, settling, and selecting individual layers of the final solution. Several methods, such as scanning electron microscopy (SEM), X-ray diffraction (XRD), thermal gravimetry (TG), differential scanning calorimetry (DSC), Fourier-transform infrared (FTIR) spectroscopy, have been used to characterize pure substances and to study the structure and thermal behavior of the composites. It was established that PVP macromolecules could both intercalate in the interlayer space of Mt and form exclusively exfoliated Mt. In addition, under certain conditions, Mt flocculated with PVP can be obtained. It is shown that during intercalation, PVP macromolecules displace and replace montmorillonite water in the interlayer space of clay mineral.

© 2023 The Author(s). Published by Elsevier B.V. on behalf of King Saud University. This is an open access article under the CC BY-NC-ND license (<http://creativecommons.org/licenses/by-nc-nd/4.0/>).

1. Introduction

Polymer nanocomposites based on layered silicates, such as Mt, still attract considerable attention because they show a sharp improvement in mechanical, thermal, barrier properties, and fire resistance with a small content of nanofiller (Dulebová et al., 2017; Jamil et al., 2022; Xie et al., 2022; Moradi et al., 2023; Xu et al., 2023; Zeng et al., 2023). Unfortunately, the promising properties of the nanocomposite are usually difficult to achieve due to the high activity of the excess surface of the nanomodifier with a tendency to agglomerate (Yu et al., 2023). To improve the dispersion of the nanoadditive, various treatments are used to improve their compatibility in the polymer matrix (e.g., modifications of

the nanoparticle surface by grafting polymer monomers, thermal or chemical treatment of nanofillers) (Sun et al., 2023). Each pair polymer-nanoadditive requires an individual approach to the nanocomposite production method (Madejová et al., 2023; Zhao et al., 2023). In the case of Mt-type nanoparticles, they are most often subjected to chemical treatment to increase their compatibility with the matrix, consisting of introducing alkylammonium or alkylphosphonium salt cations between the stacks of aluminosilicate packages (Sinha Ray and Okamoto, 2003; Gao, 2004).

To understand the influence of layered silicates on the properties of the polymer matrix, it is necessary to analyze the microstructure of the silicate. The crystallite (tactoids) consists of stacks containing between 10 and 100 parallel, equally spaced silicate platelets; each platelet is approximately 200 nm in length and 1 nm in thickness. The primary particles with a major dimension of several tens of microns, generally consist of a compact stack of individual silicate crystallite (Koo et al., 2003). The input of an organic substance between the layers of packets is called intercalation, and apart from giving it an organophilic character, the additional task of this procedure is to increase the distance between the packets. At the same time, the multilayer structure of silicate is not destroyed. Better results of strengthening the nanocomposite with Mt particles are obtained if the organoclay is exfoliated, i.e., completely loses its layered structure, and polymer chains separate

* Corresponding author.

E-mail addresses: vkrasinsky82@gmail.com (V. Krasinskyi), malinowskirafal@gmail.com (R. Malinowski), krzysztof.bajer@impib.lukasiewicz.gov.pl (K. Bajer), pytlewski@ukw.edu.pl (P. Rytlewski), andrzej.miklaszewski@put.poznan.pl (A. Miklaszewski).

Peer review under responsibility of King Saud University.



Production and hosting by Elsevier

<https://doi.org/10.1016/j.arabjc.2023.105296>

1878-5352/© 2023 The Author(s). Published by Elsevier B.V. on behalf of King Saud University.

This is an open access article under the CC BY-NC-ND license (<http://creativecommons.org/licenses/by-nc-nd/4.0/>).

the nanofiller sheets. Most often, in nanocomposites, both of the above phenomena co-occur: intercalation occurs in some packets, and some have entirely stratified (exfoliated). Such a nanocomposite is called flocculated (Gao, 2004; Wu et al., 2005; Dellisanti et al., 2006; Soegijono et al., 2020).

In this work, Mt was modified with the help of a water-soluble polymer, polyvinylpyrrolidone, to use the obtained product further to get ecological nanocomposites with high operational properties, in particular, based on biodegradable polymers. Water-soluble polymers such as PVP (Gultek et al., 2001), poly(vinyl alcohol) (PVA) (Strawhecker and Manias, 2000), and poly(ethylene oxide) (PEO) (Kuppa and Manias, 2003) can easily intercalate into sodium Mt without hydrophobic treatments (Koo et al., 2003). PVP intercalates Mt (Krasinskyi et al., 2017; Krasinskyi et al., 2019a; Krasinskyi et al., 2019b; Krasinskyi et al., 2021), and this is the basis for the creation of thermoplastic nanocomposites. In addition, PVP has an initiating effect in the polymerization of hydroxyalkylene methacrylates as an active complexing agent (Bashtyk et al., 2018; Grytsenko et al., 2019; Moravskiy et al., 2019), and also participates in the formation of new polymer matrices of liquid-structured type (Suberlyak et al., 2011; Suberlyak et al., 2012).

Many works are devoted to studying nanocomposites based on Mt and PVP. Wang et al. (2012) used a nanomodifier based on PVP and Mt to significantly improve the barrier properties of polyvinylidene fluoride and filter membranes based on it. Koo et al. (2003) and Zabska et al. (2011) reported when the Mt content in PVP is up to 20% and the components are mixed in an aqueous solution, exfoliated nanocomposites are formed. With a higher range of Mt, intercalated nanocomposites are formed. Mechanical mixing, ultrasonic mixing, and ball mill mixing were used. Séquaris et al. (2000) studied the adsorption behavior of PVP on Na-Mt in diluted solutions, representative of environmental soil solution conditions. The formation of intercalated montmorillonite tactoids and the growth of basal spacing (d001) with an increase in the adsorbed PVP amount were confirmed. The formation of a polymer layer on the surface of MMT significantly affects its adsorption capacity, particularly the binding extent of anionic and neutral organic chemicals. Jianzhong et al. (2007) used cetrimonium bromide (quaternary amine) to modify Mt. The components were mixed in an aqueous solution at a temperature 80 °C using a stirrer and ultrasound. Then the resulting product was mixed with PVP in a ratio of 1:1 to obtain a nanocomposite. Mixing was done at 90 °C using a mechanical stirrer and ultrasound. In this way, an intercalated nanocomposite was obtained.

Nanocomposites containing poly(vinyl acetate) and Mt were prepared using a single emulsion polymerization with the addition of PVP (Corobea et al., 2006). Depending on the Mt/PVP ratio, the clay was dispersed in the final polymer matrix in various forms, from individual sheets to agglomerates of transformed tactoids.

New nanocomposite films based on amylose (AM) and Fe³⁺-Mt in a PVP matrix were obtained by casting from a solution (Abdollahi et al., 2020). An increase in the content of Fe³⁺-Mt improved the hydrophilic and mechanical properties of PVP/AM films and increased their thermal stability.

Choudhary and Sengwa (2012) studied of the dielectric properties of colloidal dispersions of polyethylene oxide with PVP and Mt. The direct current ionic conductivity and the real part of the permittivity of hydrocolloids increased. At the same time, the relaxation time of the electrode polarization decreased with increasing Mt concentration. These dielectric parameters depended significantly on temperature.

Nanocomposites of PVA, PVP, and Mt were prepared by mixing in a solution and then cast into films (Mondal et al., 2013). The formation of an intercalated PVA/Mt nanocomposite was established. A layered and highly intercalated PVA/PVP/Mt nanocomposite was formed in the presence of PVP. Including PVP in the PVA/Mt matrix

enhances the interaction of hydrogen bonds between PVA and Mt. It thus improves the mechanical properties and thermal stability of the nanocomposites. The presence of a bulky ester group in the PVP chain limits its intercalation. In contrast, the adsorption behavior of PVP on Mt sheets mainly leads to exfoliated Mt structures in PVA-PVP-Mt nanocomposites (Sengwa and Choudhary, 2014). At the initial addition to the PVA/PVP mixture of 1 wt% Mt primary crystal structure of the composite underwent significant changes with the formation of new alternative crystal structures. Sharp changes in the direction and character of hydrogen bonds inside the PVA crystal structure explain this. With a further increase in the content of Mt to 10 wt%, there were significantly fewer such changes in the nanocomposite structure (Choudhary et al., 2021).

Thus, intercalated and exfoliated nanocomposites can be obtained by mixing PVP with Mt. The structure of such nanocomposites primarily depends on the PVP/Mt ratio and the method of their preparation. This work aimed to develop a new and simple method of modifying Mt with PVP, which will make it possible simultaneously to obtain modified Mt with different structures.

2. Materials and methods

2.1. Materials

Montmorillonite K10, purchased from Sigma Aldrich (281522), USA, with polydisperse particles 150–300 nm in size, in the form of agglomerates 3–20 μm (SEM analysis), specific surface area of 220–270 m²/g, bulk density of 300–370 kg/m³, pH = 2.5–3.5, cation exchange capacity of 58–60 meq/100 g, charge-balancing cation K⁺ and chemical composition (wt%) SiO₂: 72.7; Al₂O₃: 16.8; Fe₂O₃: 4.9; MgO: 1.6; was used. Polyvinylpyrrolidone 10, purchased from Duchefa Biochemie (P1368), Netherlands, with a molecular weight average of 10000, a density of 1.200 kg/m³, and a bulk density from 400 to 600 kg/m³, was used to modify Mt.

2.2. Sample preparation

In the first stage, an aqueous solution with a concentration of 5 wt% of Mt is subjected to ultrasonic waves with a frequency of 40 kHz for 6–8 min in the Sonic-0.5 apparatus (Polsonic, Poland). Then, the suspension obtained in this way is treated for 25 min in an ultrasonic field and with intensive stirring, with an aqueous solution with a concentration of 20 wt% of PVP in such a way that the mass fractions of both dissolved components, i.e., Mt and PVP, are equal to 1:2, respectively. After that, the resulting mixture is separated into three layers (Fig. 1a), subjected to decantation, separation of each layer, filtration, and drying of the target products under vacuum at a temperature of 70–80 °C until complete removal of water. The layers were separated by decanting first the upper liquid layer. After that, two layers remained in the vessel - a white pasty sediment (Mt/PVP-middle) and a gray powdery sediment (Mt/PVP-bottom) (Fig. 1b, 1c). These two layers were separated by repeated dissolution, decantation, and washing of the white pasty sediment.

After drying, three products were obtained: the bottom layer (Mt/PVP-bottom) in the form of a finely dispersed light gray powder, the middle layer (Mt/PVP-middle) - in the form of a finely dispersed white powder, and the top layer (Mt/PVP-top) - in the form of a light-yellow film, which was ground to a fine powder using a WŻ-1 laboratory mill (Research Institute of the Bakery Industry, Poland). The obtained powders were additionally dried in a vacuum at 60 °C for 3–4 h before the research. The fractions yield is (relative to the total mass of dry PVP and MMT before mixing): Mt/PVP-bottom - 20–21%, Mt/PVP-middle - 34–35%, and Mt/PVP-top - 40–41%. Irreversible losses of raw materials were about

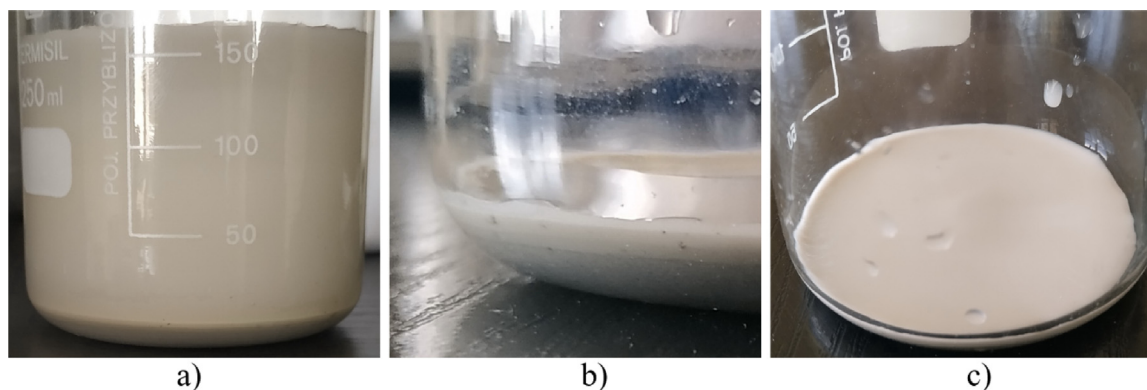


Fig. 1. The separation process of individual suspension fractions: a) three-layer suspension of Mt/PVP in water; b) after decanting the top layer; c) the middle layer (white) over the bottom layer.

3–6%. It can be assumed that the losses are mainly related to the evaporation of own moisture from hygroscopic PVP and MMT during drying of the obtained products under vacuum.

The ultrasonic waves move a given volume of the solution and produce local effects with ultrasonic frequency, ensuring high mixing speed and efficiency. This method of obtaining modified montmorillonite is environmentally friendly and highly efficient and also excludes the use of complex chemical compounds.

2.3. Sample characterization

2.3.1. X-ray diffraction (XRD)

The modified Mt and pure substances were identified via XRD. Diffraction patterns were measured on a PANalytical Empyrean diffractometer (Malvern Panalytical, Malvern, UK) with $\text{CuK}\alpha$ radiation (1.54056 Å) at a tube voltage of 45 kV and a tube current of 40 mA. The angular range was 3° to 60° with a step size of 0.017° and a counting rate of 15 s/step. Deconvolution of the reflections was performed to determine the d-value of interlayer space accurately. The Bragg equation was used to determine the d-value of interlayer space (Musiol et al., 2016). OriginPro 8 was used to analyze the acquired data.

2.3.2. Differential scanning calorimetry (DSC)

Differential scanning calorimeter, type DSC 1 STARE System (Mettler Toledo, Swiss), was used to determine the thermal properties of modified Mt and pure substances. DSC measurements were performed under nitrogen with rate flow of 50 ml/min. About 5 mg of the sample was placed on an aluminum pan for sampling. The samples were successively: heated from -40 to 300 °C at 10 °C/min, annealed at 300 °C for 3 min, cooled to -40 °C at 10 °C/min, and reheated to 300 °C at a rate of 10 °C/min. The second heating cycle was used in the analysis of the thermal properties of the studied samples.

2.3.3. Thermogravimetric analysis (TGA)

Thermogravimetric analyzer, type Q500 (TA Instruments, USA), intended for determination of thermal stability and Mt content. Thermogravimetric analysis (TGA) was performed in the temperature range of 25 – 1000 °C under a nitrogen atmosphere with a flow rate of 60 ml/min and a heating rate of 10 °C/min. The mass of the samples was about 18 mg. Before the tests, all samples were dried at 70 – 75 °C for 5 h in an air dryer.

2.3.4. Fourier-Transform infrared (FTIR) spectroscopy

Attenuated total reflectance Fourier transform infrared (ATR-FTIR) spectrometer, type Cary 630 (Agilent Technologies, USA)

meant for examination of changes in macromolecules structure. Attenuated total reflectance Fourier transform infrared (ATR-FTIR) spectra of the studied samples were recorded in absorbance mode at a constant spectral resolution of 4 cm^{-1} , for the wavenumber ranged from 3700 to 400 cm^{-1} , after acquiring 8 scans.

2.3.5. Scanning electron microscopy (SEM)

The scanning electron microscope, type Hitachi SU8010 (Hitachi, Japan), is meant to examine the microstructure of samples and the microanalysis of elements. The microstructure of the powder samples was determined by the SEM using the secondary electron (SE) detector and an accelerating voltage of 15 kV. A 5-nm thick gold layer was sputtered on all the samples to be analyzed by the SEM for better imaging quality. For that purpose, a cathode sputtering apparatus (sputter coater, type Cressington 108auto; Cressington Scientific Instruments Ltd., Germany) was used, which was equipped with a coating thickness gauge based on a quartz crystal of varying conductivity. In the case of Energy Dispersive X-ray (EDX), microanalysis of the pure substances and modified Mt samples 15 kV of accelerating voltage was applied. For EDX microanalysis, samples that were not sputtered with gold were investigated.

3. Results and discussion

3.1. Crystal structure of the modified Mt

The X-ray diffraction patterns for the modified Mt and original substances are presented in Fig. 2a–e. The diffractograms of the original MMT (Fig. 2 curve a), Mt/PVP-bottom (Fig. 2 curve b), and Mt/PVP-middle (Fig. 2 curve c) have a similar appearance. These patterns contain reflections corresponding to Mt ((001), (002), (110), (220)) and quartz ((101), (112)) (Table 1). However, the characteristic reflections intensity and position differ for these samples. In the Mt/PVP-bottom sample, all characteristic reflections shifted toward smaller 2θ angles, which increased the interlayer distance $d(001)$ to 1.100 nm compared to 1.005 nm for the original Mt (Table 1). Therefore, it can be assumed that Mt/PVP-bottom is characterized by a similar structure of two-dimensional layers as unmodified Mt; no new phases are formed, and no exfoliation occurs, but only the interlayer space increases. This is confirmed by introducing PVP macromolecules into the interlayer space of Mt, i.e., its intercalation.

In the Mt/PVP-middle sample, all characteristic reflections of Mt slightly shifted toward larger 2θ angles (Table 1). As a result, there was a slight decrease in the interlayer distance $d(001)$ by 0.006 nm. This can be explained by the removal of montmorillonite

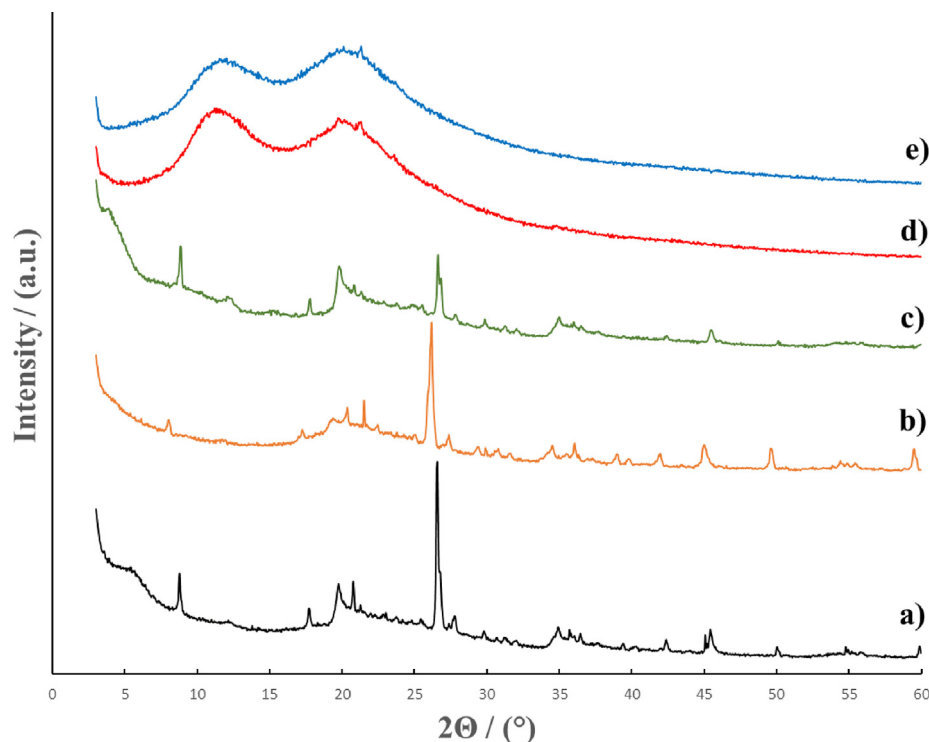


Fig. 2. X-ray diffraction patterns for Mt (a); Mt/PVP-bottom (b); Mt/PVP-middle (c); Mt/PVP-top (d), and PVP (e).

Table 1
Results of XRD analysis for modified Mt.

Reflection Index	Mt		Mt/PVP-bottom		Mt/PVP-middle		Mt/PVP-top	
	2 Θ , deg	d, nm						
M (001)	8.79	1.005	8.03	1.100	8.84	0.999	–	–
M (002)	17.71	0.500	17.06	0.519	17.81	0.498	–	–
M (110)	19.77	0.449	19.17	0.463	19.82	0.448	19.72	0.450
Q (101)	26.59	0.335	26.04	0.342	26.64	0.334	–	–
M (220)	34.91	0.257	34.41	0.260	35.01	0.256	34.81	0.258
Q (112)	45.44	0.199	44.95	0.202	45.49	0.199	–	–

water from the interlayer space and the intercalation of a smaller amount of PVP there. Such differences in the structure of Mt/PVP-middle and Mt/PVP-bottom are explained by different amounts of PVP in the samples (see Section 3.2). In addition, a significant decrease in the intensity of the Q(101) reflection at $2\Theta = 26.64^\circ$ and its splitting into two reflections can be observed on the diffractogram, as well as the disappearance of individual reflections characteristic of the original Mt. Therefore, it can be assumed that such Mt is flocculated by PVP macromolecules. That is, Mt/PVP-middle is characterized by a partially layered structure with the introduction of PVP macromolecules into the interlayer space (intercalation) and a partially exfoliated structure with separation of Mt sheets by PVP chains.

The diffractogram of the Mt/PVP-top sample (Fig. 2 curve d) is similar to the diffractogram of the original PVP (Fig. 2 curve e). However, in this sample, the reflection at $2\Theta = 20.12^\circ$, which is characteristic of PVP, disappears, and minor reflections M(110) at $2\Theta = 19.72^\circ$ and M(220) at $2\Theta = 34.81^\circ$, which are characteristic of the original Mt, appear. It is worth noting that these two reflections are shifted to the region of smaller 2Θ angles compared to the reflection of the original Mt (Table 1). The absence of the M(001) reflection at $2\Theta = 8.79^\circ$ on the Mt/PVP-top diffractogram, which characterizes the interlayer space in Mt and several other

characteristic reflections of Mt, indicates complete exfoliation of Mt and separation of Mt sheets by PVP chains. It can be assumed that there is a small amount of exfoliated Mt in the Mt/PVP-top sample since the intensity of the Mt reflections in the diffractogram is low.

3.2. Thermal degradation of the modified Mt samples

TGA was used to study the intercalation effect of Mt, the results of which are presented in Table 2 and Fig. 3. The mass loss rate (DTG) of the samples was also recorded (Fig. 4). The thermal decomposition of the original Mt occurs in three stages (Fig. 3 curve a and Table 2). In the 25–150 °C, hygroscopic and interlayer water is removed with a loss of 9.3% of the sample mass. In the temperature range of 150–512 °C, the mass loss of the sample is 2.4% and is associated with the removal of hydroxyl water from the Mt crystal lattice. Upon further heating the sample to 980 °C, the Mt crystal lattice is destroyed, and its dehydration is completed. The sample mass loss at this stage is 2.3%.

The mass loss of Mt/PVP-bottom (Fig. 3 curve b) and Mt/PVP-middle (Fig. 3 curve c) samples up to a temperature of 150 °C is significantly lower than that of pure Mt and is 3.1% and 5.3%, respectively. This indicates that in these samples, montmorillonite water

Table 2
Results of TG/DTG analysis for modified Mt samples.

Sample	Temperature range, °C	Mass loss, %	Mass residue, %
Mt	25–150	9.3	90.7
	150–512	2.4	88.3
	512–980	2.3	86
Mt/PVP-bottom	25–150	3.1	96.9
	150–512	6.6	90.3
	512–980	4.1	86.2
Mt/PVP-middle	25–150	5.3	94.7
	150–512	14.8	79.9
	512–980	8.9	71.0
Mt/PVP-top	25–95	7.1	92.9
	95–345	3.9	89.0
	345–486	80.8	8.2
	486–980	4.2	4.0
	PVP	25–85	8.5
PVP	85–350	2.3	89.2
	350–486	86.9	2.3
	486–800	2.3	0

in the interlayer space was replaced by PVP macromolecules, which are destroyed at much higher temperatures. Intensive destruction of a pure PVP sample occurs at temperatures above 350 °C (Table 2, Fig. 3 curve e and Fig. 4 curve e). Significant mass loss of Mt/PVP-bottom (6.6%) and Mt/PVP-middle (14.8%) samples in the temperature range of 150–512 °C confirms the presence of PVP macromolecules in the interlayer space of MMT. The mass loss of pure Mt in this range is only 2.4%. The higher rate and more significant mass loss of the Mt/PVP-middle sample (Fig. 4 curve c and Table 2) compared to pure Mt, and Mt/PVP-bottom in the temperature range of 150–512 °C may indicate that in this sample, in addition to intercalation, there was partial exfoliation of Mt sheets by PVP chains. Thermal destruction of such PVP chains occurs faster than intercalated (interlayer) ones. In addition, after heating to 1000 °C, the mass residues of the Mt and Mt/PVP-bottom samples are the same and amount to about 86%, while the mass residue of Mt/PVP-middle is significantly lower and is 71%. This indicates a substantially higher amount of PVP in the Mt/PVP-middle sample.

Such data confirm the intercalation of Mt by PVP macromolecules in the Mt/PVP-bottom sample and its flocculation in the Mt/PVP-middle sample. The obtained results correlate well with the results of the XRD analysis. It is worth noting that the Mt/PVP-bottom and Mt/PVP-middle samples are characterized by a more significant mass loss than the Mt sample in the temperature range of 512–980 °C indicating easier dehydroxylation of Mt layers after modification with PVP.

The TG/DTG curves of Mt/PVP-top and pure PVP samples are similar (Fig. 3 curve d and Fig. 3 curve e, Fig. 4 curve d and Fig. 4 curve e, respectively). Thermal destruction of these samples occurs during four stages (Table 2). These samples lose mass most intensively in the temperature range of 345–486 °C. However, the mass loss of samples at this stage is different and amounts to 80.8% for Mt/PVP-top and 86.9% for pure PVP. Upon further heating to 1000 °C, PVP burns completely, and the mass residue of Mt/PVP-top is 4.0%. That is, it can be stated that the content of exfoliated Mt in the Mt/PVP-top sample is about 4 wt%.

The results of TGA (Table 2) and EDX (Table 4) indicate that the highest amount of the initial PVP is in the sample Mt/PVP-top and is about 93–96 wt%, in the sample Mt/PVP-middle the content of PVP is approximately 19–22 wt%, and in the sample Mt/PVP-bottom – about 4–6 wt%. The different PVP content in separate fractions of Mt-suspension contributed to different sedimentation rates of Mt particles (Séguaris et al., 2000). As a result, three types of modified Mt structures were obtained.

3.3. FTIR spectra of the modified Mt samples

The FTIR spectra of the original Mt powder, pure PVP, and Mt samples modified with PVP are compared in Fig. 4 in the region of 3700–400 cm^{-1} . The non-intense broad band of Mt at 3640 cm^{-1} (Fig. 5 curve a) corresponds to the interlayer hydroxyl stretching ($\nu\text{Si-OH}$) (Tonle et al., 2009; Ahmed et al., 2018). The broad band at 3400 cm^{-1} and the minor band at 1633 cm^{-1} have been assigned respectively to the stretching (νOH) and bending (δOH) modes of absorbed water. The band at 798 cm^{-1} are attrib-

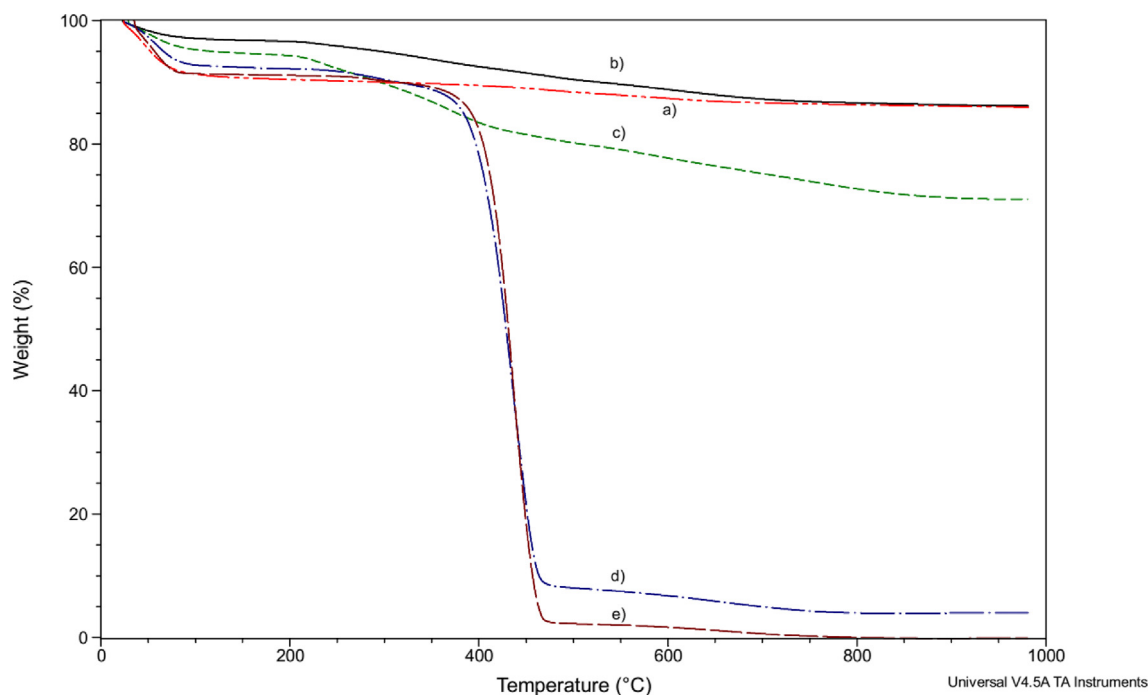


Fig. 3. TGA of Mt (a); Mt/PVP-bottom (b); Mt/PVP-middle (c); Mt/PVP-top (d), and PVP (e).

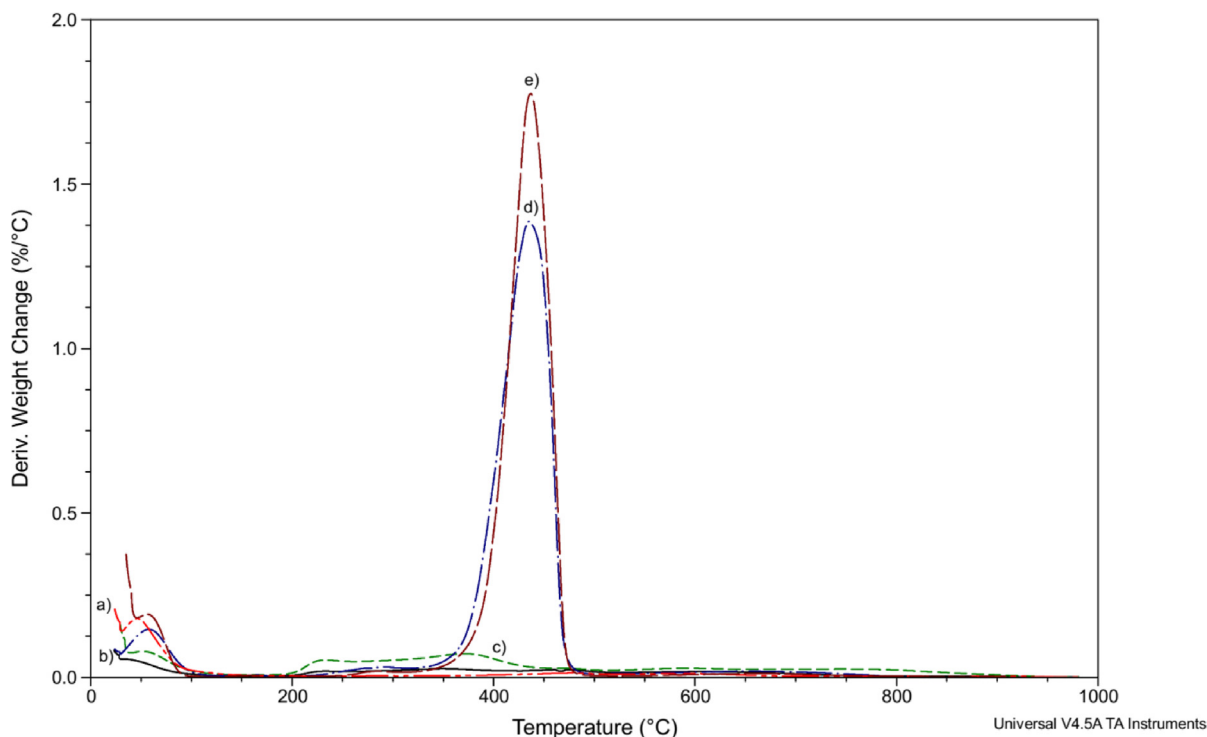


Fig. 4. DTG analyses of Mt (a); Mt/PVP-bottom (b); Mt/PVP-middle (c); Mt/PVP-top (d), and PVP (e).

uted to Si–O stretching vibrations, whereas the bands at 1032 and 451 cm^{-1} originate from the Mt Si–O–Si stretching and deformation vibrations. The band at 910 cm^{-1} corresponds to the Al–Mg–OH stretching. The band at 522 cm^{-1} corresponds to Al–O–Si vibrations associated with aluminosilicate packets in the disturbed muscovite structure (Gubernat and Zambrzycki,

2021). The weak band at 622 cm^{-1} corresponds to coupled Al–O and Si–O out-of-plane vibrations (Kim et al., 2006; Ahmed et al., 2018).

FTIR spectra of Mt/PVP-bottom (Fig. 5 curve b) and Mt/PVP-middle (Fig. 5 curve c) samples are similar to the spectrum of the original Mt. The spectrum of the Mt/PVP-top sample (Fig. 5 curve

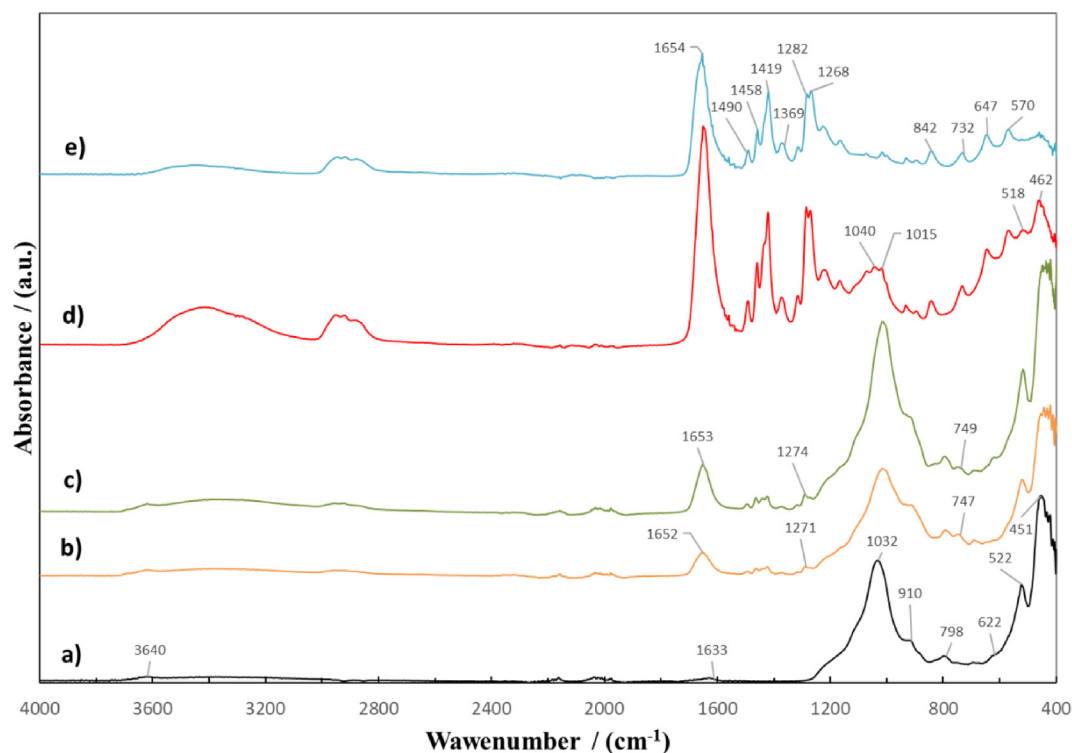


Fig. 5. ATR-FTIR spectra of Mt (a); Mt/PVP-bottom (b); Mt/PVP-middle (c); Mt/PVP-top (d), and PVP (e).

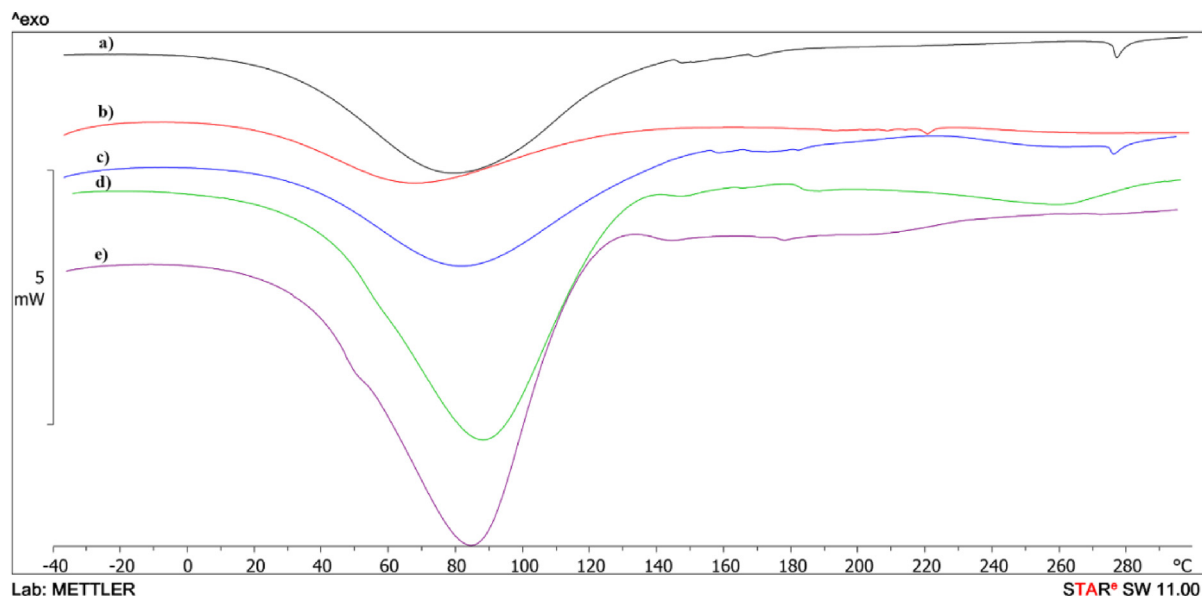


Fig. 6. DSC curves of the first heating of Mt (a); Mt/PVP-bottom (b); Mt/PVP-middle (c); Mt/PVP-top (d), and PVP (e).

d) is identical to the spectrum of pure PVP (Fig. 5 curve e). Such results correlate well with the XRD analysis and confirm the conclusions made earlier regarding the structure of the obtained samples of modified Mt. However, new absorption bands appeared at 1652 and 1653, 747, 749 cm^{-1} , and 1300–1500 cm^{-1} , characteristic of PVP (Fig. 5 curve e). The absorption band at 1652 cm^{-1} (on the pure PVP spectra – 1654 cm^{-1}) is characteristic of the stretching vibrations of the cyclic amide group in the structure of the lactam of the PVP heterocycle, as the band at 1271 cm^{-1} (on the pure PVP spectra – 1282 cm^{-1}) is characteristic of planar deformation vibrations of the C–H bond in the PVP structure (Baganizi et al., 2017; Krasinskyi et al., 2021). The relative intensity of these absorption bands (relative to the absorption band at 749–747 cm^{-1} , which is the same for both samples) is higher for the Mt/PVP-middle sample, which indicates a higher amount of PVP in this sample and correlates well with the TGA results. In addition, the spectra of the Mt/PVP-bottom and Mt/PVP-middle samples have bathochromic shifts of the absorption bands at 1032, 798, 522, and 451 cm^{-1} , which are characteristic of the original Mt. The absorption band at 1032 cm^{-1} in the Mt/PVP-bottom sample appears at 1016 cm^{-1} , and in the Mt/PVP-middle sample at 1015 cm^{-1} , the 798 cm^{-1} band in the Mt/PVP-bottom sample appears at 793 cm^{-1} , and in the Mt/PVP-middle sample at 795 cm^{-1} , the 522 cm^{-1} band in the Mt/PVP-bottom sample appears at 521 cm^{-1} , and in the Mt/PVP-middle sample at 517 cm^{-1} , the 451 cm^{-1} band in the Mt/PVP-bottom sample appears at 443 cm^{-1} , and in the Mt/PVP-middle sample at 448 cm^{-1} . Therefore, it can be stated that in the Mt/PVP-bottom and Mt/PVP-middle samples, water molecules in the interlayer space of Mt and water molecules adsorbed by montmorillonite are replaced by PVP macromolecules with subsequent physical interaction of PVP with Mt.

In contrast to the spectrum of pure PVP, the spectrum of the Mt/PVP-top has three absorption bands with shifts that are characteristic of Mt, namely a split band at 1015–1040 cm^{-1} (on the pure Mt spectra – 1032 cm^{-1}), a band at 518 cm^{-1} (on the pure Mt spectra – 522 cm^{-1}) and a band at 462 cm^{-1} (on the pure Mt spectra – 451 cm^{-1}). In addition, the spectrum of Mt/PVP-top has hypsochromic and bathochromic shifts of all absorption bands characteristic of PVP. In particular, the band at 1654 cm^{-1} shifted to

1650 cm^{-1} (bathochromic shift), and the band at 1282 cm^{-1} shifted to 1285 cm^{-1} (hypsochromic shift). The results confirm the presence in the Mt/PVP-top sample of exfoliated Mt plates, separated between PVP macromolecules and connected to them by physical bonds.

3.4. Differential scanning calorimetry

Modified Mt and original substances were investigated by the DSC method. The thermogram of the first heating of a sample of pure Mt (Fig. 6 curve a) has a well-defined endotherm in the temperature range of 30–130 °C ($\Delta H = 162.8 \text{ J/g}$) with a peak at 79 °C (Table 3), which is associated with the evaporation of adsorbed water from the surface and multilayer structure of Mt. Upon further heating of the sample, two minor *endo*-peaks are observed at 169 °C ($\Delta H = 0.3 \text{ J/g}$) and 277 °C ($\Delta H = 1.6 \text{ J/g}$), which shift to 181 °C ($\Delta H = 0.6 \text{ J/g}$) and 264 °C ($\Delta H = 0.9 \text{ J/g}$) during the second scan (Fig. 7 curve a and Table 3), respectively. These *endo*-peaks are most likely due to the subsequent evaporation of interlayer water and partial evaporation of hydroxyl water of the Mt crystal lattice, as confirmed by TGA data.

On the thermogram of the first heating of the pure PVP (Fig. 6 curve e and Table 3), there is an endotherm associated with the release of absorbed water from the PVP sample in the range of 34–120 °C ($\Delta H = 359.1 \text{ J/g}$) with a peak at 84.6 °C. This endotherm is absent upon repeated heating (Fig. 7 curve e). The glass transition temperature of the PVP sample is recorded on the DSC curve during the second scan ($T_g = 142 \text{ °C}$). No melting or crystallization peaks are observed in the heating curves of the PVP sample and in the cooling curve, indicating the original PVP's amorphous structure. The cooling curves of the samples are not presented in the article, since there are no physical transitions on them.

The *endo*-effects of evaporation of absorbed water in the temperature range of 27–148 °C are also present on the thermograms of the first scan of the samples Mt/PVP-bottom (Fig. 6 curve b), Mt/PVP-middle (Fig. 6 curve c) and Mt/PVP-top (Fig. 6 curve d). However, the values of the enthalpies of these processes differ significantly – for Mt/PVP-bottom $\Delta H = 88.6 \text{ J/g}$, for Mt/PVP-middle $\Delta H = 160.5 \text{ J/g}$ and Mt/PVP-top $\Delta H = 281.2 \text{ J/g}$ (Table 3). This indicates a different amount and type of water evaporated from these

Table 3
Results of DSC analysis for modified Mt samples.

Sample	T, °C	ΔH , J/g	Stage (process)
Mt	30–130	162.8	Evaporation of absorbed water
	169–175	0.3	Evaporation of interlayer water
	275–281	1.6	Evaporation of hydroxyl water
Mt/PVP-bottom	27–148	88.6	Evaporation of absorbed water
	179	–	Transition of PVP to a highly elastic state
Mt/PVP-middle	30–140	160.5	Evaporation of absorbed water
	161	–	Transition of PVP to a highly elastic state
	181–252	13.5	Redox processes in PVP macromolecules
Mt/PVP-top	28–126	281.2	Evaporation of absorbed water
	144	–	Transition of PVP to a highly elastic state
	218–286	16.9	Destruction of the fluctuation network
PVP	34–120	359.1	Evaporation of absorbed water
	142	–	Transition to a highly elastic state

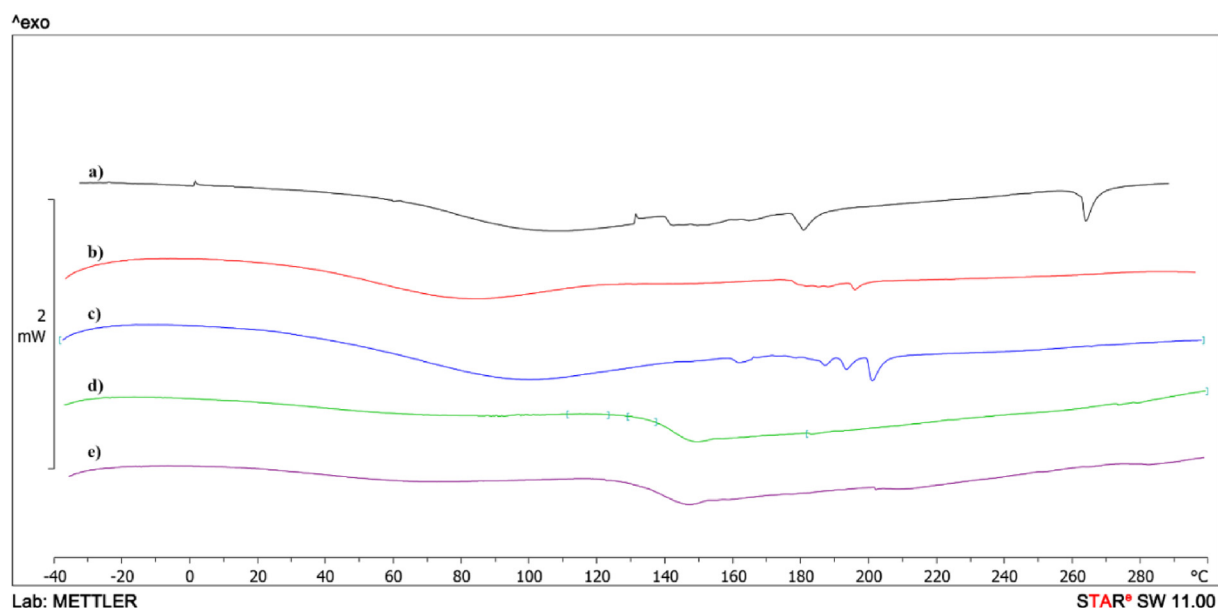


Fig. 7. DSC curves of the second heating of Mt (a); Mt/PVP-bottom (b); Mt/PVP-middle (c); Mt/PVP-top (d), and PVP (e).

samples and is consistent with the TGA data (Table 2). Upon further heating, the Mt/PVP-top sample, a blurred endotherm with a peak at 260 °C ($\Delta H = 16.9$ J/g) is observed on the thermogram, most likely associated with the partial destruction of the fluctuation network formed between PVP macromolecules and layered sheets Mt. On repeated scanning, this endotherm is absent. On the thermogram of the first heating of the Mt/PVP-middle sample, a blurred *exo*-effect is observed in the temperature range of 181–252 °C ($\Delta H = 13.5$ J/g), which disappears upon repeated heating and is absent on the thermograms of the remaining samples. Redox processes in PVP macromolecules that did not intercalate in the interlayer space of Mt or did not form a fluctuating network with partially exfoliated Mt sheets can explain this *exo*-effect. On the thermogram of the first scan of pure PVP, a very blurred *exo*-effect can be observed in this temperature region. That is, it can be concluded that redox processes occur more intensively in individual PVP macromolecules under the influence of Mt during heating to high temperatures. On the thermograms of the second heating of the Mt/PVP-bottom (Fig. 7 curve b), Mt/PVP-middle (Fig. 7 curve c), and Mt/PVP-top (Fig. 7 curve d) samples, their glass transition temperatures can be recorded, which are 179 °C, 161 °C, and 144 °C (Table 3), respectively. As we can see, the glass transition temperature of PVP in the Mt/PVP-bottom sample increases by

37 °C, in the Mt/PVP-middle sample by 19 °C, and the Mt/PVP-top sample by only 2 °C. Such results are an additional confirmation of the previously expressed assumptions about obtaining an intercalated structure in the Mt/PVP-bottom sample, a flocculated structure in the Mt/PVP-middle sample, and a completely exfoliated structure with a small amount of Mt in the Mt/PVP-top sample.

3.5. Surface morphology and composition

The surface morphology of the original substances and the modified Mt was studied using SEM (Fig. 8), and EDX analysis was also carried out (Table 4). The Mt sample has the form of poly-disperse particles in forming agglomerates (Fig. 8a). Mt has a thin layer structure with some interlayer spaces. After modification with PVP in an aqueous solution under the influence of ultrasound, the Mt structure changed. The Mt/PVP-bottom sample has a similar multilayer structure (Fig. 8b), but the sizes of the Mt sheets increased. This is due to the intercalation of PVP polymer chains into the Mt multilayer structure. The Mt/PVP-middle sample has a more porous structure, with partial exfoliation of the Mt sheets covered with PVP (Fig. 8c). The Mt/PVP-top sample has a completely exfoliated structure in which the Mt sheets are wholly cov-

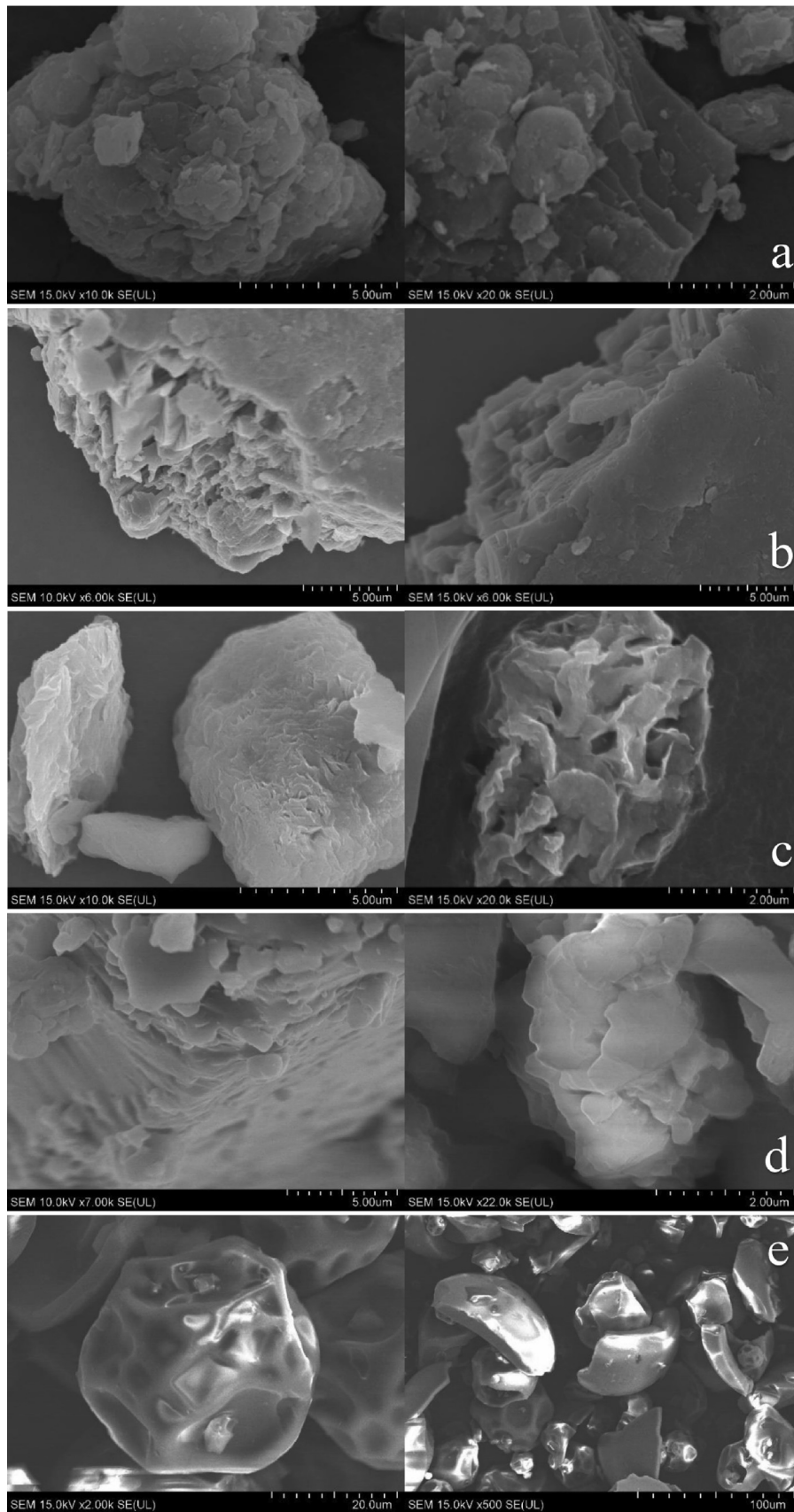


Fig. 8. SEM images of Mt (a); Mt/PVP-bottom (b); Mt/PVP-middle (c); Mt/PVP-top (d), and PVP (e).

Table 4
EDX elemental compositions of modified Mt.

Element	Elemental content, wt%				
	Mt	Mt/PVP-bottom	Mt/PVP-middle	Mt/PVP-top	PVP
C	1.85	6.96	30.36	41.15	42.99
O	45.51	51.45	35.27	30.76	29.18
Si	31.83	25.87	18.39	4.18	–
N	–	2.66	5.71	21.97	27.83
Al	10.23	6.99	5.16	1.36	–
Fe	2.38	1.80	1.36	0.25	–
Na	0.70	0.61	0.52	0.08	–
Mg	0.88	0.53	0.42	–	–
K	6.62	3.13	2.81	0.25	–

ered with PVP (Fig. 8e). The original PVP consists of polydisperse particles ranging in size from 10 to 50 μm (Fig. 8e).

The main elements in pure MMT are O (45.51%), Si (31.83%), Al (10.23%), K, Fe, Mg, Na, and C are also present in the sample (Table 4). A sample of pure PVP contains only three elements – C (42.99%), O (29.18%), and N (27.83%). All samples of modified Mt contain elements included in pure Mt and pure PVP, but the content of these elements differs significantly. This indicates a different amount of initial components in the samples of modified Mt. The lowest amount of PVP is in the Mt/PVP-bottom sample, and the highest is in the Mt/PVP-top sample. Such results correlate well with the results of XRD and TGA.

4. Conclusions

In this work, a new and straightforward method of Mt modification was developed, which consists in mixing, under the influence of ultrasound, aqueous colloidal solutions of Mt and PVP (in a ratio of Mt to PVP as 1 to 2) and selecting individual fractions that are formed during the settling of the resulting solution. As a result, three types of environmentally friendly nanomodifiers with different structures can be received from one prepared solution. The formation of intercalated Mt in the modified solution's lower (deposited) layer, flocculated Mt in the middle layer of the solution, and exfoliated Mt in the upper layer of the solution was confirmed using XRD, TG, FTIR-ATR, DSC, and SEM analyses. It was also established that each of the obtained samples of modified Mt (Mt/PVP-bottom, Mt/PVP-middle, and Mt/PVP-top) contains a different amount of PVP. The most significant amount is in the upper layer of the modified solution. The glass transition temperature of PVP in each of the nanocomposites is different; in the Mt/PVP-bottom sample, it increases by 37 $^{\circ}\text{C}$, in the Mt/PVP-middle sample by 19 $^{\circ}\text{C}$, and the Mt/PVP-top sample by only 2 $^{\circ}\text{C}$. The results of FTIR-ATR analysis confirm the presence of physical interaction between Mt and PVP in all obtained samples of modified Mt.

The main advantages of the developed method of Mt modification are its environmental friendliness (it does not require the use of any toxic chemicals; only a biocompatible water-soluble polymer was used - low molecular weight PVP, which is used in medicine), simplicity (does not require the use of complex or specific equipment), high productivity (from one of the solution, three types of nanomodifiers can be obtained at once) and relatively low irreversible losses of raw materials (in the range of 3–6%). The yield of each product is established.

Each type of modified Mt can be further used to modify polymers, including biodegradable ones, to obtain nanocomposites for various purposes. Preliminary studies of the influence of intercalated and flocculated Mt on some properties of the biopolymer polybutylene succinate (PBS) were carried out to obtain biodegradable packaging. Samples of flat films based on PBS and modified Mt were obtained. It can be argued that intercalated and flocculated

Mt affect the MFR of PBS, increase the tearing strength of the films, and significantly improve the optical and mechanical properties of the film. Moreover, this effect is different from the effect of pure Mt on these characteristics of PBS. The following works will be devoted to a detailed study of such biodegradable nanocomposites.

Funding

The project has been financed by the own funds of Łukasiewicz Research Network – Institute for Engineering of Polymer Materials and Dyes.

CRedit authorship contribution statement

Volodymyr Krasinskyi: Conceptualization, Methodology, Investigation, Writing – original draft, Visualization. **Rafał Malinowski:** Conceptualization, Methodology, Resources, Writing – review & editing. **Krzysztof Bajer:** Supervision, Resources, Writing – review & editing. **Piotr Rytlewski:** Investigation, Resources. **Andrzej Miklaszewski:** Investigation, Resources, Writing – review & editing.

Declaration of Competing Interest

The authors declare that they have no known competing financial interests or personal relationships that could have appeared to influence the work reported in this paper.

References

- Abdollahi, R., Orang, N.S., Afkhami, F.A., Khandar, A.A., Mahmoudi, G., Hayati, P., Zubkov, F.I., 2020. Effect of Fe^{3+} -MMT nanocomposite content on thermal, mechanical and water resistance behavior of PVP/Amylose Films. *Polym. Bull.* 77, 6491–6508. <https://doi.org/10.1007/s00289-019-03083-5>.
- Ahmed, A., Chaker, Y., Belarbi, E.H., Abbas, O., Chotard, J.N., Abassi, H.B., Van Nhien, A.N., El Hadri, M., Bresson, S., 2018. XRD and ATR/FTIR investigations of various montmorillonite clays modified by monocationic and dicationic imidazolium ionic liquids. *J. Mol. Struct.* 1173, 653–664. <https://doi.org/10.1016/j.molstruc.2018.07.039>.
- Baganizi, D., Nyairo, E., Duncan, S., Singh, S., Dennis, V., 2017. Interleukin-10 conjugation to carboxylated PVP-coated silver nanoparticles for improved stability and therapeutic efficacy. *Nanomaterials* 7 (7), 165. <https://doi.org/10.3390/nano7070165>.
- Bashtyk, Y., Fechan, A., Grytsenko, O., Hotra, Z., Kremer, I., Suberlyak, O., Aksimentyeva, O., Horbenko, Y., Kotsarenko, M., 2018. Electrical elements of the optical systems based on hydrogel - electrochromic polymer composites. *Mol. Cryst. Liq. Cryst.* 672 (1), 150–158. <https://doi.org/10.1080/15421406.2018.1550546>.
- Choudhary, S., Sengwa, R.J., 2012. Dielectric properties of PEO-PVP-MMT nanocomposite hydrocolloids. *Indian J. Phys.* 86 (5), 335–340. <https://doi.org/10.1007/s12648-012-0063-9>.
- Choudhary, S., Dhatarwal, P., Sengwa, R.J., 2021. Study on crystalline phases and degree of crystallinity of the melt compounded PVA/MMT and PVA/PVP/MMT nanocomposites. *Indian J. Pure Appl. Phys.* 59 (2), 92–102. <https://doi.org/10.56042/ijpap.v59i2.45457>.
- Corobea, M.-C., Uricanu, V., Donescu, D., Deladi, S., Radovici, C., Serban, S., Constantinescu, E., 2006. Variable morphologies of poly(vinyl acetate)-montmorillonite nanocomposites obtained by emulsion polymerization in the presence of poly(vinyl pyrrolidone). *E-Polymers* 6 (1). <https://doi.org/10.1515/epoly.2006.6.1.767>.
- Dellisanti, F., Minguzzi, V., Valdrè, G., 2006. Thermal and structural properties of CA-rich montmorillonite mechanically deformed by compaction and Shear. *Appl. Clay Sci.* 31 (3–4), 282–289. <https://doi.org/10.1016/j.clay.2005.09.006>.
- Dulebová, L., Greškovič, F., Sikora, J.W., Krasinskyi, V., 2017. Analysis of the mechanical properties change of PA6/MMT nanocomposite system after ageing. *Key Eng. Mater.* 756, 52–59. <https://doi.org/10.4028/www.scientific.net/kem.756.52>.
- Gao, F., 2004. Clay/Polymer composites: the story. *Mater. Today* 7 (11), 50–55. [https://doi.org/10.1016/s1369-7021\(04\)00509-7](https://doi.org/10.1016/s1369-7021(04)00509-7).
- Grytsenko, O.M., Pukach, P.Y., Suberlyak, O.V., Moravskiy, V.S., Kovalchuk, R.A., Bereznyy, B.V., 2019. The SCHEFFE's method in the study of mathematical model of the polymeric hydrogels composite structures optimization. *Math. Model. Comput.* 6 (2), 258–267. <https://doi.org/10.23939/mmc2019.02.258>.
- Gubernat, M., Zambrzycki, M., 2021. Catalytic activity of K10 Montmorillonite in the chemical vapor deposition of multi-wall carbon nanotubes from methane. *Appl. Clay Sci.* 211. <https://doi.org/10.1016/j.clay.2021.106178>.

- Gultek, A., Seckin, T., Onal, Y., Icduygu, M.G., 2001. Preparation and phenol capturing properties of polyvinylpyrrolidone-montmorillonite hybrid materials. *J. Appl. Polym. Sci.* 81 (2), 512–519. <https://doi.org/10.1002/app.1465>.
- Jamil, M., Elouahli, A., Abida, F., Assaoui, J., Gourri, E., Hatim, Z., 2022. APATITIC calcium phosphate/montmorillonite nano-biocomposite: In-situ synthesis, characterization and dissolution properties. *Heliyon* 8 (8), e10042.
- Jianzhong, M., Dangge, G., Bin, L., Yun, C., Jianfang, D., 2007. Study on PVP/C-MMT nanocomposite material via Polymer Solution-intercalation method. *Mater. Manuf. Process.* 22 (6), 715–720. <https://doi.org/10.1080/10426910701385283>.
- Kim, N.H., Malhotra, S.V., Xanthos, M., 2006. Modification of cationic nanoclays with ionic liquids. *Microporous Mesoporous Mater.* 96 (1–3), 29–35. <https://doi.org/10.1016/j.micromeso.2006.06.017>.
- Koo, C.M., Ham, H.T., Choi, M.H., Kim, S.O., Chung, I.J., 2003. Characteristics of polyvinylpyrrolidone-layered silicate nanocomposites prepared by attrition ball milling. *Polymer* 44, 681–689. [https://doi.org/10.1016/s0032-3861\(02\)00803-0](https://doi.org/10.1016/s0032-3861(02)00803-0).
- Krasinskyi, V., Kochubei, V., Klym, Y., Suberlyak, O., 2017. Thermogravimetric research into composites based on the mixtures of polypropylene and modified polyamide. *Eastern-Eur. J. Enterprise Technol.* 4 (12), 44–50. <https://doi.org/10.15587/1729-4061.2017.108465>.
- Krasinskyi, V., Gajdos, I., Suberlyak, O., Antoniuk, V., Jachowicz, T., 2019a. Study of the structure and thermal characteristics of nanocomposites based on polyvinyl alcohol and intercalated Montmorillonite. *J. Thermoplast. Compos. Mater.* 34 (12), 1680–1691. <https://doi.org/10.1177/0892705719879199>.
- Krasinskyi, V., Suberlyak, O., Zemke, V., Klym, Y., Gaidos, I., 2019b. The role of polyvinylpyrrolidone in the formation of nanocomposites based on a compatible polycaprolactam and polypropylene. *Ch&ChT* 13 (1), 59–63. <https://doi.org/10.23939/chct13.01.059>.
- Krasinskyi, V., Suberlyak, O., Sikora, J., Zemke, V., 2021. Nanocomposites based on polyamide-6 and montmorillonite intercalated with polyvinylpyrrolidone. *Polym.-Plastics Technol. Mater.* 60 (15), 1641–1655. <https://doi.org/10.1080/25740881.2021.1924201>.
- Kuppa, V., Manias, E., 2003. Dynamics of poly(ethylene oxide) in nanoscale confinements: a computer simulations perspective. *J. Chem. Phys.* 118 (7), 3421–3429. <https://doi.org/10.1063/1.1538601>.
- Madejová, J., Barlog, M., Slaný, M., Bashir, S., Scholtzová, E., Tunega, D., Jankovič, L., 2023. Advanced materials based on montmorillonite modified with poly(ethylenimine) and poly(2-methyl-2-oxazoline): Experimental and DFT Study. *Colloids Surf. A Physicochem. Eng. Asp* 659. <https://doi.org/10.1016/j.colsurfa.2022.130784>.
- Mondal, D., Mollick, M.M., Bhowmick, B., Maity, D., Bain, M.K., Rana, D., Mukhopadhyay, A., Dana, K., Chattopadhyay, D., 2013. Effect of poly(vinyl pyrrolidone) on the morphology and physical properties of poly(vinyl alcohol)/sodium montmorillonite nanocomposite films. *Prog. Nat. Sci.: Mater. Int.* 23 (6), 579–587. <https://doi.org/10.1016/j.pnsc.2013.11.009>.
- Moradi, Z., Alihosseini, A., Ghadami, A., 2023. Adsorption removal of arsenic from aqueous solution by carboxy methyl cellulose(cmc) modified with montmorillonite. *Results Mater.* 17. <https://doi.org/10.1016/j.rinma.2023.100378>.
- Moravskiy, V.S., Levytskyi, V.Y., Masyuk, A.S., Bilyi, L.M., Humenets'kyi, T.V., 2019. Influence of modified condensed foamed polystyrene on the morphology and properties of polycaprolactam. *Mater. Sci.* 54 (6), 836–842. <https://doi.org/10.1007/s11003-019-00271-6>.
- Musiol, P., Szatkowski, P., Gubernat, M., Weselucha-Birczynska, A., Blazewicz, S., 2016. Comparative study of the structure and microstructure of pan-based nano- and micro-carbon fibers. *Ceram. Int.* 42 (10), 11603–11610. <https://doi.org/10.1016/j.ceramint.2016.04.055>.
- Sengwa, R.J., Choudhary, S., 2014. Structural characterization of hydrophilic polymer blends/montmorillonite clay nanocomposites. *J. Appl. Polym. Sci.* 131 (16). <https://doi.org/10.1002/app.40617>.
- Séguaris, J.M., Hild, A., Narres, H.D., Schwuger, M.J., 2000. Polyvinylpyrrolidone adsorption on Na-montmorillonite. Effect of the polymer interfacial conformation on the colloidal behavior and binding of chemicals. *J. Colloid Interface Sci.* 230 (1), 73–83. <https://doi.org/10.1006/jcis.2000.7046>.
- Sinha Ray, S., Okamoto, M., 2003. Polymer/layered silicate nanocomposites: A review from preparation to processing. *Prog. Polym. Sci.* 28 (11), 1539–1641. <https://doi.org/10.1016/j.progpolymsci.2003.08.002>.
- Soegijono, B., Chanra, J., Zhongwu, Z., Mi, P., 2020. Synthesis polymer styrene butadiene hybrid latex with laponite organoclay as filler via emulsion polymerization technique for application in paper coating. *ARPN J. Eng. Appl. Sci.* 15 (22), 2673–2687.
- Strawhecker, K.E., Manias, E., 2000. Structure and properties of poly(vinyl alcohol)/na+ montmorillonite nanocomposites. *Chem. Mater.* 12 (10), 2943–2949. <https://doi.org/10.1021/cm000506g>.
- Suberlyak, O., Krasinskyi, V., Sikora, J., Krzyżak, A., 2012. Ammonia-free, low-toxic press-materials with improved electroinsulating properties based on modified Novolak phenol-formaldehyde resin. *Ch&ChT* 6 (2), 199–202. <https://doi.org/10.23939/chct06.02.199>.
- Suberlyak, O.V., Krasinskyi, V.V., Shapoval, I.M., Hrytsenko, O.M., 2011. Influence of the mechanism and parameters of hardening of modified Novolak phenol-formaldehyde resins on the physicomechanical properties of the composite. *Mater. Sci.* 46 (5), 669–678. <https://doi.org/10.1007/s11003-011-9339-z>.
- Sun, W., Zhang, T., Li, J., Zhu, X., 2023. Enhanced gaseous acetone adsorption on montmorillonite by ball milling generated si-oh and interlayer under synergistic modification with H₂O₂ and tetramethylammonium bromide. *Chemosphere* 321. <https://doi.org/10.1016/j.chemosphere.2023.138114>.
- Tonle, I.K., Letaief, S., Ngameni, E., Detellier, C., 2009. Nanohybrid materials from the grafting of imidazolium cations on the interlayer surfaces of kaolinite. application as electrode modifier. *J. Mater. Chem.* 19 (33), 5996–6003. <https://doi.org/10.1039/b907401e>.
- Wang, P., Ma, J., Wang, Z., Shi, F., Liu, Q., 2012. Enhanced separation performance of PVDF/PVP-g-MMT nanocomposite ultrafiltration membrane based on the NVP-grafted polymerization modification of montmorillonite (MMT). *Langmuir* 28 (10), 4776–4786. <https://doi.org/10.1021/la203494z>.
- Wu, D., Zhou, C., Yu, W., Fan, X., 2005. Effect of flocculated structure on rheology of poly(butylene terephthalate)/clay nanocomposites. *J. Polym. Sci. B* 43, 2807–2818. <https://doi.org/10.1002/polb.20568>.
- Xie, G., Xiao, Y., Bai, Y., Luo, Y., Wang, R., Gu, S., 2022. Synthesis of alkyl polyamine with different functional groups and its montmorillonite swelling inhibition mechanism: experiment and density functional theory simulation. *Appl. Clay Sci.* 230. <https://doi.org/10.1016/j.clay.2022.106715>.
- Xu, J., Wang, X., Chen, J., Ding, T., Xue, J., 2023. Inhibition mechanism of cationic polyacrylamide on Montmorillonite Surface Hydration: a molecular dynamics simulation study. *Chem. Phys.* 567. <https://doi.org/10.1016/j.chemphys.2022.111792>.
- Yu, J., Zhang, P., Zhang, Y., Sun, K., Shi, X., Li, L., 2023. The preparation of conjugated microporous polymer composite materials with montmorillonite template and its improvement in photocatalytic degradation for multiple antibiotics. *Appl. Clay Sci.* 231. <https://doi.org/10.1016/j.clay.2022.106752>.
- Zabska, M., Jaskiewicz, K., Kiersnowski, A., Szustakiewicz, K., Rathgeber, S., Piglowski, J., 2011. Spontaneous exfoliation and self-assembly phenomena in polyvinylpyrrolidone/synthetic layered silicate nanocomposites. *Radiat. Phys. Chem.* 80 (10), 1125–1128. <https://doi.org/10.1016/j.radphyschem.2011.02.019>.
- Zeng, Z.L., Yu, C., Liao, R.P., Cai, X., Chen, Z.H., Yu, Z., Wu, Z.X., 2023. Preparation and characterization of sodium polyacrylate grafted montmorillonite nanocomposite for the adsorption of cadmium ions from aqueous solution. *Colloids Surf. A Physicochem. Eng. Asp* 656. <https://doi.org/10.1016/j.colsurfa.2022.130389>.
- Zhao, Y., Lai, J., Huang, Y., Jiang, H., Sun, Y., Li, Y., Li, Y., Li, F., Luo, Z., Xie, D., 2023. Effect of molding on the structure and properties of poly(butylene adipate-terephthalate)/poly(propylene carbonate)/organically modified montmorillonite nanocomposites. *Appl. Clay Sci.* 234. <https://doi.org/10.1016/j.clay.2023.106854>.